A field-pilot for passive bioremediation of As-rich acid mine drainage

L. Fernandez-Rojo, C. Casiot, E. Laroche, V. Tardy, O. Bruneel, S. Delpoux, A. Desoeuvre, G. Grapin, J. Savignac, J. Boisson, et al.

*Title page

A field-pilot for passive bioremediation of As-rich acid mine drainage

Fernandez-Rojo L.[a,1], Casiot C.[a*], Laroche E.[a,b], Tardy V.[a,2], Bruneel O.[a], Delpoux S.[a], Desoeuvre A.[a], Grapin G.[c], Savignac J.[c], Boisson J.[d], Morin G.[e], Battaglia-Brunet F.[b], Joulian C.[b], Héry M.[a]

[a] *HydroSciences Montpellier, Univ. Montpellier, CNRS, IRD, 163 rue Auguste Broussonnet, 34090 Montpellier, France*

[b] *French Geological Survey (BRGM), Geomicrobiology and environmental monitoring unit, 3, avenue Claude Guillemin, BP 36009, 45060 Orléans Cedex 2, France*

[c] *IRH Ingénieur Conseil, Anteagroup, 427 rue Lavoisier - CS 50155, 54714, Ludres Cedex, France*

[d] *IRH Ingénieur Conseil, Anteagroup, 197 avenue de Fronton, 31200, Toulouse, France*

[e] *Institut de Minéralogie, de Physique des Matériaux et de Cosmochimie (IMPMC), UMR 7590 CNRS-UPMC-IRD-MNHN, Sorbonne Universités, 4 place Jussieu, 75252 Paris cedex 05, France*

*Author for correspondence: Corinne Casiot

Tel +33 (0)4 67 14 33 56
Email: casiot@msem.univ-montp2.fr
Postal address: Université de Montpellier, Hydrosciences - CC57, 163 rue Auguste Broussonnet, 34090 Montpellier, France

Declarations of interest: none

[1] Present address: Institute of Environmental Assessment and Water Research (IDAEA), CSIC, Jordi Girona 18, 08034 Barcelona, Spain

[2] Present address: Irstea UR Milieux Aquatiques, Ecologie et Pollutions (UR MALY) – Irstea – 5 rue de la Doua BP 32108 F-69616 Villeurbanne Cedex, France

Abstract

A field-pilot bioreactor exploiting microbial iron (Fe) oxidation and subsequent arsenic (As) and Fe co-precipitation was monitored during 6 months for the passive treatment of As-rich acid mine drainage (AMD). It was implemented at the Carnoulès mining site (southern France) where AMD contained 790–1315 mg L^{-1} Fe(II) and 84–152 mg L^{-1} As, mainly as As(III) (78 – 83 %). The bioreactor consisted in five shallow trays of 1.5 m^2 in series, continuously fed with AMD by natural flow. We monitored the flow rate and the water physico-chemistry including redox Fe and As speciation. Hydraulic retention time (HRT) was calculated and the precipitates formed inside the bioreactor were characterized (mineralogy, Fe and As content, As redox state). Since As(III) oxidation improves As retention onto Fe minerals, bacteria with the capacity to oxidize As(III) were quantified through their marker gene *aioA*. Arsenic removal yields in the pilot ranged between 3 % to 97 % (average rate $(1.8 \pm 0.8) \times 10^{-8}$ mol L^{-1} s^{-1}), and were positively correlated to HRT and inlet water dissolved oxygen concentration. Fe removal yields did not exceed 11 % (average rate $(7 \pm 5) \times 10^{-8}$ mol L^{-1} s^{-1}). In the first 32 days, the precipitate contained tooeleite, a rare arsenite ferric sulfate mineral. Then, it evolved toward an amorphous ferric arsenate phase. The As/Fe molar ratio and As(V) to total As proportion increased from 0.29 to 0.86 and from ~20 % to 99 %, respectively. The number of bacterial *aioA* gene copies increased ten-fold during the first 48 days and stabilized thereafter. These results and the monitoring of arsenic speciation in the inlet and the outlet water, provide evidences that As(III) oxidized in the pilot. The biotreatment system we designed proved to be suitable for high As DMA.

The formation of sludge highly enriched into As(V) rather than As(III) is advantageous in the perspective of long term storage.

Keywords: field bioreactor, passive treatment, As(III) oxidation, amorphous ferric arsenate, tooeleite, arsenic removal rate

1. Introduction

Acid Mine Drainage (AMD) is one of the worst environmental hazards resulting from the extraction of base metals from sulfide deposits. These leachates result from the oxidation of metal sulfides (especially pyrite) in mine tailings. The process releases sulfate, iron and a range of toxic metals and metalloids, often including arsenic. This element can be present at high concentrations in AMD, up to 350 mg L^{-1} (Paikaray, 2015; Williams, 2001). Arsenic contamination may be attenuated to some extent by natural processes which involve biotic and abiotic Fe(II) oxidation and the subsequent precipitation of Fe(III)-hydroxysulfates and Fe(III)-oxyhydroxides, together with arsenite (As(III)) and arsenate (As(V)) adsorption and/or co-precipitation (Cheng et al., 2009). The oxidation of arsenite into arsenate, which is efficiently mediated by bacteria (Battaglia-Brunet et al., 2002; Bruneel et al., 2003) greatly improves As attenuation in AMD. Indeed, the solubility of As(V)-Fe(III)-hydroxysulfates is lower than the solubility of As(III)-Fe(III)-hydroxysulfates for a similar As/Fe ratio in the solid (Maillot et al., 2013). These natural processes can serve as a basis for the passive treatment of As-rich AMD if they are exploited in suitable systems. Passive treatments, that do not require neither power nor constant maintenance, are particularly adapted to

remote locations. Numerous studies aimed to exploit microbial Fe(II) oxidation for the removal of As from AMD in lab-scale bioreactors processing synthetic mine water (e.g. Ahoranta et al., 2016; González-Contreras et al., 2012; Hedrich and Johnson, 2014). Conversely, few trials have been attempted to exploit this process in field-pilot passive bioreactors processing real AMD water (Elbaz-Poulichet et al., 2006; Macías et al., 2012; Whitehead et al., 2005) (Table 1).

In the present study, we investigated arsenic removal from an AMD containing extreme As concentrations (up to 140 mg L^{-1}) under the most mobile and toxic form, As(III) (60–100 %, Casiot et al., 2003). The treatment consisted in a passive field-pilot bioreactor exploiting iron oxidation by autochthonous bacterial communities, resulting in the precipitation of Fe and As. The design of this reactor was derived from previous laboratory experiments with a bench-scale channel bioreactor that provided up to 80 % As removal during the treatment of AMD water originating from the same site (Fernandez-Rojo et al., 2017). The two key parameters of the bioreactor design were 1) a low water height above the precipitate and 2) a good oxygenation of the feed water (Fernandez-Rojo et al., 2017). The field-pilot bioreactor was continuously fed during six months with AMD by natural flow. The AMD was the spring of the Reigous Creek at the Carnoulès mine in southern France (OREME, 2018), whose biogeochemistry and microbial communities involved in Fe and As attenuation have been previously studied (Bruneel et al., 2006,2011; Casiot et al., 2003; Egal et al., 2010; Volant et al., 2014). We monitored inlet and outlet water physico-chemistry and the composition of Fe-As precipitate, including arsenic redox state in water and precipitate. To estimate potential microbial contribution to arsenite oxidation, the gene encoding the large subunit of the As(III) oxidase (*aioA*) was quantified.

2. Materials and methods

2.1. Field-scale passive bioreactor

A flow pipe collected the AMD from its spring, located at the base of the Carnoulès tailings dam, and transferred it to the bioreactor, located 115 m down the way (mean slope of 5.9 %). At the bioreactor inlet, a small feed tank (52 cm length × 21 cm width × 26 cm height) limited the flow rate entering the bioreactor by means of a V-notch weir and a siphon. The level of water in the V-notch weir tank was constant and it was adjustable by the height of the siphon. The overflow was redirected to the Reigous Creek through a flow pipe (Figure 1A). The inlet flow rate decreased over short time intervals (~ one to two weeks) due to the inflow of sand particles into the AMD carrying pipes. Thus, cleaning these pipes was necessary after each sampling survey to restore the flow rate. Besides, a decantation tank was inserted upstream from the AMD intake after day 147 to limit the introduction of sand particles into the pipe.

Water circulation within the bioreactor was powered by natural flow. The bioreactor consisted of five shallow trays stacked head to tail on a shelf (Figure 1). Each tray sized 1.5 m^2 (1.5 × 1 m), 0.11 m depth, and it was made of 10 mm thick polyethylene sheets. Trays were divided into two compartments with a vertical separator leaving a 2 cm space at the bottom. The main compartment (1.2 × 1 m) was filled 3.5–4.5 cm in height with 80 kg of sand from river Moselle (uniformity coefficient 5.73, diameter at 10 % = 0.31 mm, at 60 % = 1.78 mm, at 85 % = 5.75 mm, $CaCO_3$ content = 0.19 %), in order to provide a support for microbial attachment. The overflow fell over from the outlet end of one tray to the inlet end of the next tray, through a polypropylene tube (2 cm i.d.),

thus favoring the water oxygenation. Water passed through the different trays (T1, T2, T3, T4 and T5) before being discharged to the AMD stream.

2.2. Monitoring

The bioreactor was monitored during 194 days, between June 10th 2016 and December 21st 2016. Nine sampling surveys were made during the summer period (June, July), one intermediate sampling in October, and four samplings during the autumn period (November, December). At each sampling campaign, inlet and outlet waters were collected. The following physico-chemical parameters were measured: pH, dissolved oxygen concentration (DO), temperature, redox potential (Eh) and electrical conductivity (EC). We also determined dissolved concentrations of Fe(II), total Fe, As(III), As(V), and total As, after filtration (0.22 µm) and preservation using procedures described in Fernandez-Rojo et al. (2017). We measured the flow rate and the water height in each tray in order to estimate the apparent hydraulic retention time (HRT). The apparent HRT was the mean of the maximum and the minimum HRT. To determine the maximum HRT, we assumed that water flowed through the sand pores and that there was no precipitate accumulation. On the contrary, for minimum HRT determination, we considered that the sand pores were clogged and that there was a precipitate layer above the sand.The maximum and the minimum HRT, expressed in hours, were calculated with the following Equation (1):

$$Maximum/Minimum\ HRT = \frac{\sum_{i=1}^{n}(L_i * W_i) * (WH_i - PH_i) - \left(\frac{SW_i}{\delta} - \emptyset_i\right)}{Q} \qquad (1)$$

where "L_i" and "W_i" were the length and the width, respectively, in decimeters. "WH_i" was the water height from the bottom of one tray measured in each sampling in decimeters. "PH_i" was the precipitate height above the sand layer of one tray expressed in decimeters. "SW_i" was the sand weight in kg, "δ" was the sand density in kg dm^{-3}, "ø" was the sand vacuum volume in dm^3, and "Q" the water flow rate in dm^3 h^{-1}. "n" corresponded to the number of trays (5) in the pilot. Details of these calculations are given in the supporting information file.

2.3. Analyses

2.3.1. *Water samples*

All analytical procedures are detailed in Fernandez-Rojo et al. (2017). Briefly, the concentrations of dissolved Fe(II) were determined using colorimetry at 510 nm after complexation with 1,10-phenanthrolinium chloride. Total dissolved concentrations of Fe, As and other elements (S (SO_4^{2-}), Al, Zn, and Pb) were determined using ICP-MS. Arsenic redox speciation was determined using HPLC-ICP-MS.

The rates of Fe(II) oxidation, Fe- and As-removal (in mol L^{-1} s^{-1}) were calculated using Equation (2):

$$\text{Rate} = \frac{([X]inlet - [X]outlet)}{HRT} \quad (2)$$

where [X] was the concentration of dissolved Fe(II), total dissolved Fe, total dissolved As, dissolved As(III) or dissolved As(V), respectively, in mol L^{-1} and HRT the apparent hydraulic retention time in seconds.

Surface area is often a limitation in the design of passive treatments. To address this issue and to compare with the literature data on water treatment processes (Table 1), area-adjusted rates were calculated using Equation 3:

$$\text{Area} - \text{adjusted rate} = \frac{([X]inlet - [X]outlet) * Q}{Surface\ area} \quad (3)$$

where the concentration of total dissolved Fe or total dissolved As ([X]) were expressed in g L^{-1}, the flow rate (Q) in L d^{-1} and the surface area, in m^2. Only the 7.5 m^2 surface above the sand layer was considered here because rapid clogging prevented water to circulate through the sand layer.

2.3.2. *Solid samples*

When sampling the precipitate, the surface of each tray was divided in three zones following the water flow path (Figure 1A): "A" refers to the 0.5 m^2 surface area close to the inlet of each tray, "B" represents the 0.5 m^2 surface area in the middle section, and "C" the 0.5 m^2 surface area close to the outlet of each tray. The precipitate from trays T1 to T5 was collected with a sterilized spatula by scraping the solid surface. The precipitate was transferred into Falcon Tubes (50 mL) and centrifuged for 10 min at 4400 × g (Sorwall ST40, Thermo Scientific). The supernatant was discarded and the precipitate was homogenized. A portion of the sample (~0.3 g) was dried in a vacuum desiccator. Redox As determination was performed by HPLC-ICP-MS on a subsample

(100 mg) after extraction with orthophosphoric acid (Resongles et al., 2016). No fine particles remained after this procedure, enabling total As and Fe determination. Another subsample was used for X-ray diffraction (XRD) and a third one for quantification of *aioA* gene copy numbers. These procedures were detailed in Fernandez-Rojo et al. (2017).

2.4. Statistics

Friedman tests and Nemenyi post-hoc tests were performed with the XLSTAT 2018 software to compare the As/Fe molar ratio, the As(V)% and the number of *aioA* genes/ng of DNA of the biogenic precipitate between the sampling dates.

Principal Component Analysis (PCA) was performed on functional parameters of the pilot (As and Fe removal yields and rates) using the vegan package under R software (version 3.4.0) and provided an ordination of data in factorial maps based on the scores of the first two principal components. HRT and water physico-chemistry (inlet and outlet temperature and DO, pH, Eh, conductivity, Fe and As concentration, Fe(II) to total Fe proportion, As(III) to total As proportion) were fit to PCA ordinations in order to identify the correlations between these variables and the functional parameters of the pilot.

3. Results

3.1. Flow rate and hydraulic retention time

The HRT calculation relies mainly on the flow rate. This parameter exhibited important variations, from 6 to 130 L h^{-1} in relation with partial clogging of the pipe carrying the

AMD to the bioreactor feed tank (Figure 2). The October survey (day 115) was characterized by extremely low flow rate occurring after a two-month period without flow pipe dredging. After day 147, a decantation tank was set up, resulting in a better stabilization of the flow rate, between 30 and 49 L h^{-1}. The HRT calculation also relies on the water height measured from the bottom of the trays. This parameter varied between 34 and 112 mm. Indeed, the accumulation of precipitate within and over the sand bed modified water discharge at the outlet of each tray, which subsequently increased the water level within the tray. Consequently, the calculated apparent HRT varied from 4 h to ~50 h (Figure 2).

3.2. Water physico-chemistry

3.2.1. *Inlet water*

Inlet water pH, DO and temperature exhibited notable variations over the monitoring period (Figure 3). pH varied between 2.6 and 3.4 (Figure 3A). Dissolved oxygen concentration was generally lower than 4 mg L^{-1} during the summer period (except on day 45) and increased to 5.2 ± 0.3 mg L^{-1} in the autumn period (Figure 3B). The water temperature was higher during the summer period (19 ± 3 °C) than during the autumn period (11 ± 1 °C) (Figure 3C). Eh averaged 539 ± 30 mV (Figure 3D). Total dissolved Fe and As concentrations increased respectively from 962 mg L^{-1} to 1314 mg L^{-1} and from 111 to 152 mg L^{-1} during the summer period and then decreased to 801 ± 81 mg L^{-1} (Fe) and 92 ± 10 mg L^{-1} (As) in the autumn period (Figure 3E-F). Both elements were predominantly under the reduced redox state (more than 84 % Fe(II) and 78 % As(III) (Figure S1B-D)). Dissolved sulfate and metal cations (Al, Zn, Pb)

concentrations in the inlet water averaged 2.8 ± 0.5 g L^{-1} (SO_4^{2-}), 47 ± 7 mg L^{-1} (Al), 21 ± 3 mg L^{-1} (Zn) and 1.5 ± 0.3 mg L^{-1} (Pb), respectively (Figure S1E-H).

3.2.2. *Outlet water*

There was a decrease of pH up to 0.4 unit in the outlet water compared to the inlet (Figure 3A). Water temperature between inlet and outlet varied within ± 4°C during summer period, while a decrease (up to 7.3 °C) was always observed during the autumn period (Figure 3C). Dissolved oxygen most systematically increased, by 5 mg L^{-1} at most, between inlet and outlet (except on day 45). Fe removal yield did not exceed 11 % (Figure 3E) and up to 20 % Fe(II) was oxidized (Figure S1B)). Arsenic removal yield ranged from 3 % to 97 % (Figure 3F). The corresponding removal rates varied from 5.7 × 10^{-9} to 1.6 × 10^{-7} mol L^{-1} s^{-1} for Fe (average rate 7 ± 5 ×10^{-8} mol L^{-1} s^{-1}) and from 1 ×10^{-8} to 3.2 ×10^{-8} mol L^{-1} s^{-1} for As (average rate 1.8 ± 0.8 ×10^{-8} mol L^{-1} s^{-1}) (Figure 4). Reduced Fe(II) and As(III) species remained predominant upon oxidized species in the outlet water (more than 85% Fe(II) and 74% As(III)). The October data (day 115) was an exception, with 98 % As(V) in the outlet water. Concentrations of dissolved Al, Zn, S (SO_4^{2-}) and Pb also decreased between inlet and outlet, by less than 12 % for Al, Zn, S and up to 45 % for Pb (Figure S1 E-H).

PCA illustrates the relationships between the functional parameters of the pilot (As and Fe removal yields and rates) and the operating conditions including HRT and physico-chemical variables (Figure 5). Days 115 to 194 (autumn period) were characterized by the highest As removal yields, which were significantly correlated to HRT (p-value < 0.001) and to inlet water DO concentration (p-value = 0.006). Days 11, 27 and

32 were characterized by the highest Fe removal yields, which were negatively correlated (p-value = 0.025) to the proportion of Fe(II) to total Fe in inlet water.

3.3. Biogenic precipitate: mineralogy, molar As/Fe ratios, As redox state and *aioA* gene quantification

The precipitate recovered on the top of the sand layer contained quartz, mica, and potassium feldspar all originating from the sand filter material (Figure 6). The Fe and As content stabilized to 179 ± 39 mg Fe g^{-1} and 152 ± 33 mg As g^{-1} after 48 days (Table S1). Tooeleite, a ferric arsenite sulfate mineral ($Fe_6(AsO_3)_4SO_4(OH)_4.4H_2O$) was the only crystallized Fe-As phase identified. The XRD pattern also evidenced an amorphous phase whose proportion increased at the expense of tooeleite, during the monitoring period (Figure 6). The molar As/Fe ratio in the precipitate significantly increased during the monitoring period from ~0.3 to ~0.7 in the three trays analyzed (Figure 7A). The proportion of As(V) upon total As in the precipitate also increased from ~20 % to ~85 % during the first 50 days, and then remained constant around nearly 100 % until the end of the monitoring period (Figure 7B). The color of the precipitate changed throughout time, from orange to pale yellow (Figure S2).

The relative abundance of arsenite oxidizing bacteria was assessed through the quantification of *aioA* genes. A ten-fold increase of the number of *aioA* genes was observed in the precipitate between day 11 and day 48. From this date, the number of *aioA* genes remained relatively stable until the end of the monitoring period (Figure 7C).

4. Discussion

4.1. Arsenic and iron removal efficiency in the field-scale bioreactor

The field pilot removed 3 % to 97 % of total dissolved As from the Carnoulès AMD, while Fe removal yield did not exceed 11 %. The HRT had a significant influence on As removal yields; the important variations of HRT during the monitoring period are both due to flow rate fluctuations and to water level variations inside the trays. The average As removal rate ($(1.8 \pm 0.8) \times 10^{-8}$ mol L^{-1} s^{-1}) was close to our lab-scale experiments rates (2×10^{-8} to 5×10^{-8} mol L^{-1} s^{-1}) (Fernandez-Rojo et al., 2017). For comparison, in a laboratory bioreactor exploiting microbial Fe(II) oxidation, Ahoranta et al. (2016) obtained an As removal rate of ~ 1.5×10^{-10} mol L^{-1} s^{-1} during the treatment of a synthetic AMD containing 10 mg L^{-1} As(III) by adsorption onto biogenic jarosite at pH 3. Numerous factors, including water physico-chemistry, nature of precipitated solids, and microbial communities might influence As removal rate in AMD (Asta et al., 2010, 2012). The Fe removal rate ($(7 \pm 5) \times 10^{-8}$ mol L^{-1} s^{-1}) in the field pilot was within the lower range of lab-scale experiments rates (1.8 to 24×10^{-8} mol L^{-1} s^{-1}, Fernandez-Rojo et al. (2017)). The field pilot oxidized less than 20 % Fe(II) whatever the HRT (Figure S1-B), compared to nearly 100 % in the lab-scale pilot (Fernandez-Rojo et al., 2017). There was no link between Fe removal yield and HRT or inlet water DO (Figure 5). Thus, the system appeared not very effective regarding Fe oxidation and removal. One possible explanation is the large water height (15–70 mm) above the precipitate. We demonstrated in our lab-scale bioreactor that large water height limits oxygen availability (and then Fe(II) oxidation and subsequent Fe precipitation) at the

water/precipitate interface, due to faster metabolic consumption, relative to the oxygen diffusion (Fernandez-Rojo et al., 2017).

A few *in situ* devices exploiting microbial or abiotic Fe(II) oxidation have been experienced so far for arsenic removal in AMD in a passive way (Table 1). They were in the form of ponds (Elbaz-Poulichet et al., 2006), lagoons (Macías et al., 2012) or wetlands (Hamilton et al., 1999; Whitehead et al., 2005). Some of them were preceded by closed or open channels or drains filled with alkaline rocks (Caraballo et al., 2009; Gusek et al., 1994; Rötting et al., 2008) in order to promote rapid abiotic Fe(II) oxidation at near-neutral pH prior to As retention (Table 1). Most of these systems achieved more than 80 % removal for AMD containing low As concentrations (< 3 mg L^{-1}). Area-adjusted arsenic removal rates obtained in the present study were higher (3–12 g m^{-2} d^{-1}) than those described in previous studies, in relation with higher dissolved arsenic content. The high As concentration of the Carnoulès AMD is particularly challenging. In a previous field-pilot experiment in Carnoulès, only 13–20 % As removal was achieved (Elbaz-Poulichet et al., 2006). The present bioreactor showed a substantial improvement of As removal yield.

4.2. As-bearing phases formed in the pilot

Tooeleite and an amorphous-Fe-As phase were identified in the biogenic precipitate of the field-pilot. These mineral phases have been observed for years in the upstream section of Reigous Creek, in fresh and dry sediments, and in laminated concretions (Morin et al., 2003; Egal et al., 2010). These solid phases were favored upon the most widespread As-schwertmannite due to the As/Fe ratio exceeding 0.3 in the precipitate. Indeed, an As/Fe ratio higher than 0.15 was shown to disrupt the crystallization of

As(V)-schwertmannite (Carlson et al., 2002). In the field-pilot, tooeleite was replaced over time by an amorphous phase subsequently to As(V) enrichment in the precipitate (Figure 6; Table S1), consistently with the study of Liu et al. (2015). These authors found that the crystallinity of tooeleite decreased with increasing As(V)/As(III) ratio and no more tooeleite was detected on the XRD spectrum when the As(V)/As(III) ratio exceeded 0.4 (Liu et al., 2015). The latter conditions occurred after day 19 in the present experiment, with As(V)/As(III) ratio in the precipitate increasing beyond 0.7. This is consistent with the formation of an amorphous ferric arsenate phase. Future work should examine whether the characteristics of As-bearing phases (As content, As/Fe ratio and mineralogy) and their evolution over the long-term constitute limiting factors in the achievement of the lowest As concentration in the treated water.

4.3. Arsenic oxidation

As(III) was predominant (> 78 %) over As(V) in the feed water and both As(III) and As(V) species were removed from the dissolved phase in similar proportion in the bioreactor (Figure S1C-D). Conversely, As(V) was predominant (> 50 %) over As(III) in the precipitate after 20 days functioning and reached nearly one hundred percent in trays T1-C, T2-C and T5-C after 170 days (Figure 7B; Table S1). Thus, As(III) appeared to be oxidized within the field pilot. Both biotic and abiotic As(III) oxidation may be involved. Abiotic As(III) oxidation may occur in presence of dissolved Fe(III) (Asta et al., 2012; Emett and Khoe, 2001) or at the surface of Fe(III) minerals (Bhandari et al., 2011; 2012; Paikaray et al., 2014; Pozdnyakov et al., 2016; Sun and Doner, 1998) in acidic environments in presence of light. However, batch experiments conducted with AMD waters from Carnoulès showed that the photochemical oxidation was negligible

compared to the biological oxidation (Egal et al., 2009). Similar results were obtained by other authors in an acid hydrothermal discharge (Leiva et al., 2014).

Furthermore, the temporal increase of the As-oxidation genetic potential (expressed as the number of copies of *aioA* genes/ng of DNA) during the first 50 days (Figure 6C) strongly suggests the establishment of As(III)-oxidizing bacteria in the biogenic precipitate. The As(III)-oxidizing *Thiomonas* spp. have proved to be active members of the bacterial community in the Reigous Creek (Bruneel et al., 2011). They are the only arsenite oxidizers described so far in Carnoulès where they express *in situ* their arsenite oxidation activity catalyzed by the AioA enzyme (Hovasse et al., 2016). We can therefore hypothesize that arsenite oxidation occurring in the bioreactor is mainly biological.

5. Conclusion and perspectives

The present field system provided As removal at a similar rate than the lab-scale pilot. However, the water circulation in the system must be improved to stabilize the HRT in future work. Fe oxidation and precipitation yield appeared to be limited by the large water height above the precipitate. Nevertheless, the low amount of iron precipitated (maximum 11 %), compared to other systems where the AMD is neutralized, enables the production of low amounts of sludge, highly concentrated in arsenic (up to 20 % dry weight), thus limiting the cost of As-rich sludge disposal in engineered hazardous wastes landfill facilities. The nature of the As-bearing phases produced, mainly amorphous ferric arsenate, is advantageous in the perspective of long-term storage of these treatment sludges. This solid phase has a high As load and a low solubility compared to As(III)-Fe(III) phases (Langmuir et al., 2006; Virčíková et al., 1995;

Maillot et al., 2013). However, the influence of storage conditions on sludge stability needs to be fully evaluated.

Future efforts should focus on As removal rate improvement. For this, higher oxygenation should be tested, together with the introduction in the trays of a physical support with high pore volume, such as pozzolana, to prevent fast clogging and to maximize surface area of Fe-and As-oxidizing biofilm per unit of water volume (Battaglia-Brunet et al., 2006). In the perspective of upscaling of the treatment unit, long-term monitoring would be necessary to explore possible seasonal variation of the removal yields and As redox state in the precipitate. Long-term monitoring would also provide information on the frequency of sludge removal from the system. Furthermore, the spatio-temporal dynamic of bacteria involved in Fe(II) and As(III) oxidation such as *Thiomonas* spp. in the present field-scale pilot deserves further research.

This treatment could be implemented as one step targeting arsenic in a multi-step AMD treatment. Indeed, iron, sulfate and metal cations (Al, Zn, Pb) are only partially removed by this treatment and outlet pH remains acid (pH~3). A sulfate reduction bioreactor could be implemented to raise the pH and selectively recover zinc in the form of sulfide (Chen et al., 2016; Hedrich and Johnson, 2014; Le Pape et al., 2017). A finish treatment such as Dispersed alkaline substrate (DAS) and decantation ponds might be used to further raise the pH and remove remaining Fe, Al, and other metal cations, before discharge into natural water bodies (Caraballo et al., 2011, 2009; Rötting et al., 2008).

Acknowledgements

The authors thank the IngECOST-DMA project (ANR-13-ECOT-0009), the OSU OREME (SO POLLUMINE Observatory, funded since 2009) and the Ecole Doctorale

GAIA (PhD fellowship of Lidia Fernandez-Rojo, 2014-2017) for the financial support. We thank Remi Freydier and Léa Causse for ICP-MS analysis on the AETE-ISO platform (OSU OREME, University of Montpellier). We thank Pierre Marchand for his assistance in field sampling campaigns. We thank Simone Toller, from the University of Pisa, for his valuable involvement during the setup of the bioreactor. We thank Qiuwei Li, from the Université Pierre et Marie Curie, for her contribution in XRD measurements during her internship at Institut de minéralogie, de physique des matériaux et de cosmochimie (IMPMC).

References

Ahoranta, S.H., Kokko, M.E., Papirio, S., Özkaya, B., Puhakka, J.A., 2016. Arsenic removal from acidic solutions with biogenic ferric precipitates. J. Hazard. Mater. 306, 124–132. doi:10.1016/j.jhazmat.2015.12.012

Asta, M.P., Ayora, C., Acero, P., Cama, J., 2010. Field rates for natural attenuation of arsenic in Tinto Santa Rosa acid mine drainage (SW Spain). J. Hazard. Mater. 177, 1102–1111. doi:10.1016/j.jhazmat.2010.01.034

Asta, M.P., Kirk Nordstrom, D., Blaine McCleskey, R., 2012. Simultaneous oxidation of arsenic and antimony at low and circumneutral pH, with and without microbial catalysis. Appl. Geochem. 27, 281–291. doi:http://dx.doi.org/10.1016/j.apgeochem.2011.09.002

Battaglia-Brunet, F., Dictor, M.-C., Garrido, F., Crouzet, C., Morin, D., Dekeyser, K., Clarens, M., Baranger, P., 2002. An arsenic(III)-oxidizing bacterial population: selection, characterization, and performance in reactors. J. Appl. Microbiol. 93, 656–667. doi:10.1046/j.1365-2672.2002.01726.x

Battaglia-Brunet, F., Itard, Y., Garrido, F., Delorme, F., Crouzet, C., Greffie, C., Joulian, C., 2006. A simple biogeochemical process removing arsenic from a mine drainage water. Geomicrobiol. J. 23, 201–211. doi:10.1080/01490450600724282

Bhandari, N., Reeder, R.J., Strongin, D.R., 2011. Photoinduced oxidation of arsenite to arsenate on ferrihydrite. Environ. Sci. Technol. 45, 2783–2789. doi:10.1021/es103793y

Bhandari, N., Reeder, R.J., Strongin, D.R., 2012. Photoinduced oxidation of arsenite to arsenate on goehite. Environ. Sci. Technol. 46, 8044–8051. doi:/10.1021/es300988p

Bruneel, O., Personné, J.C., Casiot, C., Leblanc, M., Elbaz-Poulichet, F., Mahler, B.J., Le Flèche, A., Grimont, P.A.D., 2003. Mediation of arsenic oxidation by *Thiomonas* sp. in acid-mine drainage (Carnoulès, France). J. Appl. Microbiol. 95, 492–499. doi :10.1046/j.1365-2672.2003.02004.x

Bruneel, O., Duran, R., Casiot, C., Elbaz-Poulichet, F., Personné, J.C., 2006. Diversity of microorganisms in Fe-As-rich acid mine drainage waters of Carnoulès, France. Appl. Environ. Microbiol. 72, 551–556. doi:10.1128/AEM.72.1.551-556.2006

Bruneel, O., Volant, A., Gallien, S., Chaumande, B., Casiot, C., Carapito, C., Bardil, A., Morin, G., Brown Jr., G.E., Personné, J.C., Le Paslier, D., Schaeffer, C., Van Dorsselaer, A., Bertin, P.N., Elbaz-Poulichet, F., Arsène-Ploetze, F., 2011. Characterization of the active bacterial community involved in natural attenuation processes in arsenic-rich creek sediments. Microb. Ecol. 61, 793–810. doi:10.1007/s00248-011-9808-9

Caraballo, M.A., Rötting, T.S., Macías, F., Nieto, J.M., Ayora, C., 2009. Field multi-step limestone and MgO passive system to treat acid mine drainage with high metal concentrations. Appl. Geochem. 24, 2301–2311. doi:10.1016/j.apgeochem.2009.09.007

Caraballo, M.A., Macías, F., Rötting, T.S., Nieto, J.M., Ayora, C., 2011. Long term remediation of highly polluted acid mine drainage: A sustainable approach to restore the environmental quality of the Odiel river basin. Environ. Pollut. 159, 3613–3619. doi:10.1016/j.envpol.2011.08.003

Carlson, L., Bigham, J.M., Schwertmann, U., Kyek, A., Wagner, F., 2002. Scavenging of As from acid mine drainage by schwertmannite and ferrihydrite: a comparison with synthetic analogues. Environ. Sci. Technol. 36, 1712–1719.doi:10.1021/es0110271

Casiot, C., Morin, G., Juillot, F., Bruneel, O., Personné, J.-C., Leblanc, M., Duquesne, K., Bonnefoy, V., Elbaz-Poulichet, F., 2003. Bacterial immobilization and oxidation of arsenic in acid mine drainage (Carnoulès creek, France). Water Res. 37, 2929–2936. doi:http://dx.doi.org/10.1016/S0043-1354(03)00080-0

Chen, C.-J., Jiang, W.-T., 2012. Influence of waterfall aeration and seasonal temperature variation on the iron and arsenic attenuation rates in an acid mine drainage system. Appl. Geochem. 27, 1966–1978. doi:http://dx.doi.org/10.1016/j.apgeochem.2012.06.003

Chen, L.-X., Huang, L.-N., Méndez-García, C., Kuang, J.-L., Hua, Z.-S., Liu, J., Shu, W.-S., 2016. Microbial communities, processes and functions in acid mine drainage ecosystems. Curr. Opin. Biotechnol. 38, 150–158. doi:10.1016/j.copbio.2016.01.013

Cheng, H., Hu, Y., Luo, J., Xu, B., Zhao, J., 2009. Geochemical processes controlling fate and transport of arsenic in acid mine drainage (AMD) and natural systems. J Hazard Mater. 165, 13-26. doi: 10.1016/j.jhazmat.2008.10.070.

Egal, M., Casiot, C., Morin, G., Parmentier, M., Bruneel, O., Lebrun, S., Elbaz-Poulichet, F., 2009. Kinetic control on the formation of tooeleite, schwertmannite and jarosite by *Acidithiobacillus ferrooxidans* strains in an As(III)-rich acid mine water. Chem. Geol. 265, 432–441. doi:10.1016/j.chemgeo.2009.05.008

Egal, M., Casiot, C., Morin, G., Elbaz-Poulichet, F., Cordier, M.-A., Bruneel, O., 2010. An updated insight into the natural attenuation of As concentrations in Reigous Creek (southern France). Appl. Geochem. 25, 1949–1957. doi:http://dx.doi.org/10.1016/j.apgeochem.2010.10.012

Elbaz-Poulichet, F., Bruneel, O., Casiot, C., 2006. The Carnoulès mine. Generation of As-rich acid mine drainage, natural attenuation processes and solutions for passive in-situ remediation, in: Difpolmine (Diffuse Pollution From Mining Activities).

Emett, M.T., Khoe, G.H., 2001. Photochemical oxidation of arsenic by oxygen and iron in acidic solutions. Water Res. 35, 649–656. doi:http://dx.doi.org/10.1016/S0043-

1354(00)00294-3

Fernandez-Rojo, L., Héry, M., Le Pape, P., Braungardt, C., Desoeuvre, A., Torres, E., Tardy, V., Resongles, E., Laroche, E., Delpoux, S., Joulian, C., Battaglia-Brunet, F., Boisson, J., Grapin, G., Morin, G., Casiot, C., 2017. Biological attenuation of arsenic and iron in a continuous flow bioreactor treating acid mine drainage (AMD). Water Res. 123, 594–606. doi:10.1016/j.watres.2017.06.059

González-Contreras, P., Weijma, J., Buisman, C.J.N., 2012. Continuous bioscorodite crystallization in CSTRs for arsenic removal and disposal. Water Res. 46, 5883–5892. doi:10.1016/j.watres.2012.07.055

Gusek, J.J., Gormley, J.T., Scheetz, J.W., 1994. Design and construction aspects of pilot-scale passive treatment systems for acid rock drainage at metal mines. Hydrometallurgy 777–793. doi:10.1007/978-94-011-1214-7

Hamilton, Q.U.I., Lamb, H.M., Hallett, C., Proctor, J. a., 1999. Passive treatment systems for the remediation of acid mine drainage at Wheal Jane, Cornwall. Water Environ. J. 13, 93–103. doi:10.1111/j.1747-6593.1999.tb01014.x

Hedrich, S., Johnson, D.B., 2014. Remediation and selective recovery of metals from acidic mine waters using novel modular bioreactors. Environ. Sci. Technol. 48, 12206–12212. doi:10.1021/es5030367

Hovasse, A., Bruneel, O., Casiot, C., Desoeuvre, A., Farasin, J., Hery, M., Van Dorsselaer, A., Carapito, C., Arsène-Ploetze, F., 2016. Spatio-temporal detection of the *Thiomonas* population and the *Thiomonas arsenite oxidase* involved in natural arsenite attenuation processes in the Carnoulès acid mine drainage. Front. Cell Dev. Biol. 4, 1–14. doi:10.3389/fcell.2016.00003

Langmuir, D., Mahoney, J., Rowson, J., 2006. Solubility products of amorphous ferric arsenate and crystalline scorodite ($FeAsO_4 \cdot 2H_2O$) and their application to arsenic behavior in buried mine tailings. Geochim. Cosmochim. Acta 70, 2942–2956. doi:10.1016/j.gca.2006.03.006

Leiva, E.D., Rámila, C. d P., Vargas, I.T., Escauriaza, C.R., Bonilla, C.A., Pizarro, G.E., Regan, J.M., Pasten, P.A., 2014. Natural attenuation process via microbial oxidation of arsenic in a high Andean watershed. Sci. Total Environ. 466–467, 490–502. doi:10.1016/j.scitotenv.2013.07.009

Le Pape, P., Battaglia-Brunet, F., Parmentier, M., Joulian, C., Gassaud, C., Fernandez-Rojo, L., Guigner, J.-M., Ikogou, M., Stetten, L., Olivi, L., Casiot, C., Morin, G., 2017. Complete removal of arsenic and zinc from a heavily contaminated acid mine drainage via an indigenous SRB consortium. J. Hazard. Mater. 321, 764–772. doi:10.1016/j.jhazmat.2016.09.060

Liu, J., Deng, S., Zhao, F., Cheng, H., Frost, R.L., 2015. Spectroscopic characterization and solubility investigation on the effects of As(V) on mineral structure tooeleite ($Fe_6(AsO_3)_4SO_4(OH)_4 \cdot H_2O$). Spectrochim. Acta A Mol. Biomol. Spectrosc. 134, 428–433. doi:10.1016/j.saa.2014.06.111

Macías, F., Caraballo, M.A., Nieto, J.M., Rötting, T.S., Ayora, C., 2012. Natural pretreatment and passive remediation of highly polluted acid mine drainage. J. Environ. Manage. 104, 93–100. doi:http://dx.doi.org/10.1016/j.jenvman.2012.03.027

Maillot, F., Morin, G., Juillot, F., Bruneel, O., Casiot, C., Ona-Nguema, G., Wang, Y., Lebrun, S., Aubry, E., Vlaic, G., Brown Jr., G.E., 2013. Structure and reactivity of As(III)- and As(V)-rich schwertmannites and amorphous ferric arsenate sulfate from the Carnoulès acid mine drainage, France: comparison with biotic and abiotic model compounds and implications for As remediation. Geochim. Cosmochim. Acta 104, 310–329. doi:10.1016/j.gca.2012.11.016.

Morin, G., Juillot, F., Casiot, C., Bruneel, O., Personné, J.-C., Elbaz-Poulichet, F., Leblanc, M., Ildefonse, P., Calas, G., 2003. Bacterial formation of tooeleite and mixed arsenic(III) or arsenic(V)−iron(III) gels in the Carnoulès acid mine drainage, France. A XANES, XRD, and SEM study. Environ. Sci. Technol. 37, 1705–1712. doi:10.1021/es025688p

OREME, observatoire de l'ancien site minier de Carnoulès (2018). https://data.oreme.org/carnoules/home (accessed on November 19th 2018).

Paikaray, S., Essilfie-Dughan, J., Göttlicher, J., Pollok, K., Peiffer, S., 2014. Redox stability of As(III) on schwertmannite surfaces. J. Hazard. Mater. 265, 208–216. doi:10.1016/j.jhazmat.2013.11.068

Paikaray, S., 2015. Arsenic geochemistry of acid mine drainage. Mine Water Environ. 34, 181–196. doi:10.1007/s10230-014-0286-4

Pozdnyakov, I.P., Ding, W., Xu, J., Chen, L., Wu, F., Grivin, V.P., Plyusnin, V.F., 2016. Photochemical transformation of an iron(III)-arsenite complex in acidic aqueous solution. Photochem. Photobiol. Sci. 15, 431–439. doi:10.1039/c5pp00240k

Resongles, E., Le Pape, P., Fernandez-Rojo, L., Morin, G., Brest, J., Guo, S., Casiot, C., 2016. Routine determination of inorganic arsenic speciation in precipitates from acid mine drainage using orthophosphoric acid extraction followed by HPLC-ICP-MS. Anal. Methods 8, 7420–7426. doi:10.1039/c6ay02084d

Rötting, T.S., Caraballo, M.A., Serrano, J.A., Ayora, C., Carrera, J., 2008. Field application of calcite Dispersed Alkaline Substrate (calcite-DAS) for passive treatment of acid mine drainage with high Al and metal concentrations. Appl. Geochem. 23, 1660–1674. doi:10.1016/j.apgeochem.2008.02.023

Sun, X., Doner, H.E., 1998. Adsorption and oxidation of arsenite on goethite. Soil Sci. 163, 278–287. doi:10.1097/00010694-199804000-00003

Virčíková, E., Molnár, Ľ., Lech, P., Reitznerová, E., 1995. Solubilities of amorphous Fe-As precipitates. Hydrometallurgy 38, 111–123. doi:http://dx.doi.org/10.1016/0304-386X(94)00072-B

Volant, A., Bruneel, O., Desoeuvre, A., Héry, M., Casiot, C., Bru, N., Delpoux, S., Fahy, A., Javerliat, F., Bouchez, O., Duran, R., Bertin, P.N., Elbaz-Poulichet, F., Lauga, B., 2014. Diversity and spatiotemporal dynamics of bacterial communities: physicochemical and other drivers along an acid mine drainage. FEMS Microbiol. Ecol. 90, 247–263. doi:10.1111/1574-6941.12394

Whitehead, P.G., Hall, G., Neal, C., Prior, H., 2005. Chemical behaviour of the Wheal Jane bioremediation system. Sci. Total Environ. 338, 41–51. doi:10.1016/j.scitotenv.2004.09.004

Williams, M., 2001. Arsenic in mine waters: an international study. Environ. Geol. 40, 267–278. doi:10.1007/s002540000162

Figure 1

Click here to download Figure: 20181014_Figure 1.docx

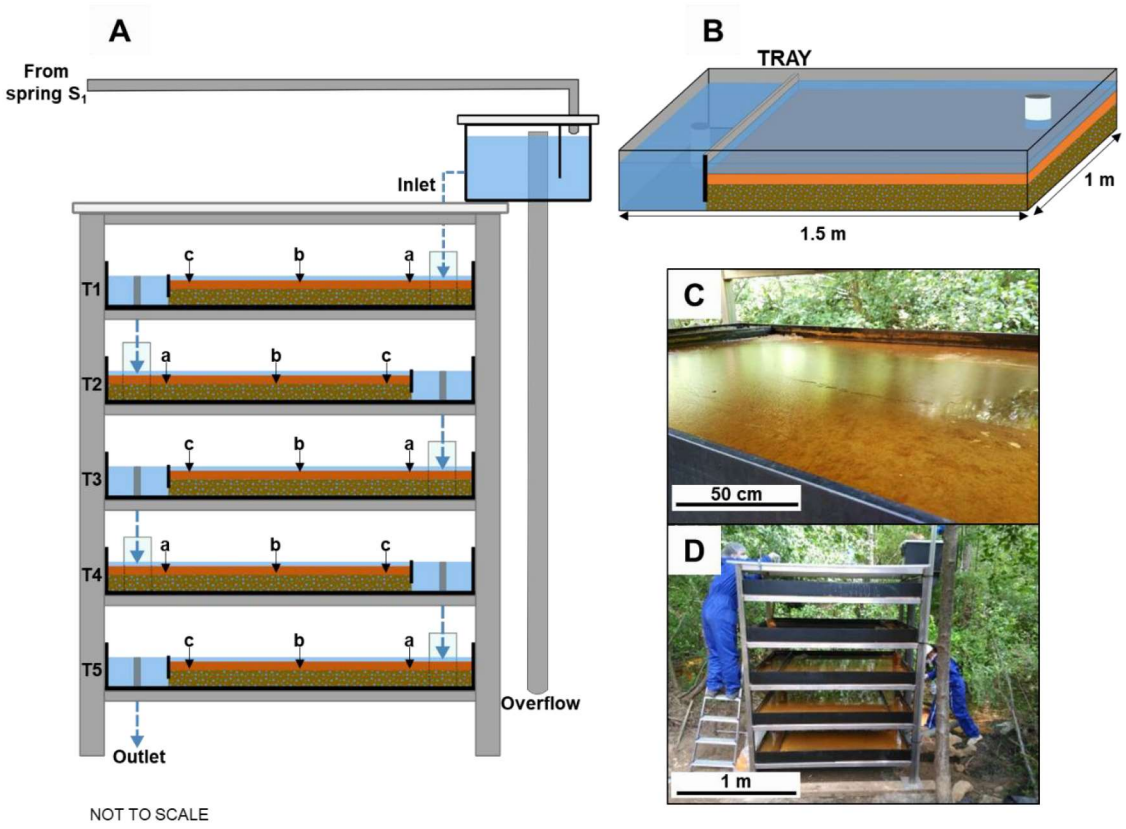

Figure 1. Schematic representation of the field bioreactor with the five trays (T = tray) (A) and detail of each tray (B). Pictures of one of the trays showing the orange biogenic precipitate below the thin water layer (C), and of the whole field bioreactor (D) from June 2016. Letters a, b and c in (A) indicate the biogenic precipitates sampling locations.

Figure 2
Click here to download Figure: 20181014_Figure 2.docx

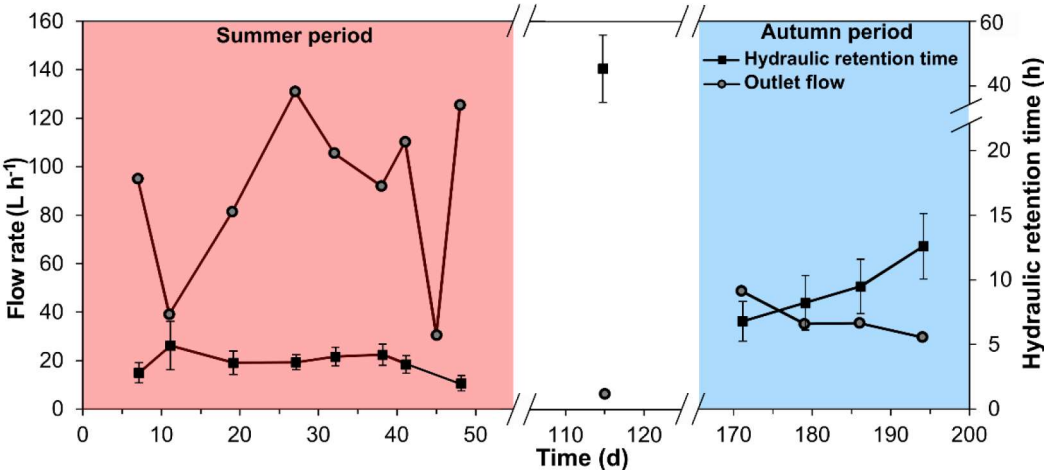

Figure 2. Variation of the flow rate during the monitoring period and estimation of the HRT.

Figure 3
Click here to download Figure: 20181014_Figure 3.docx

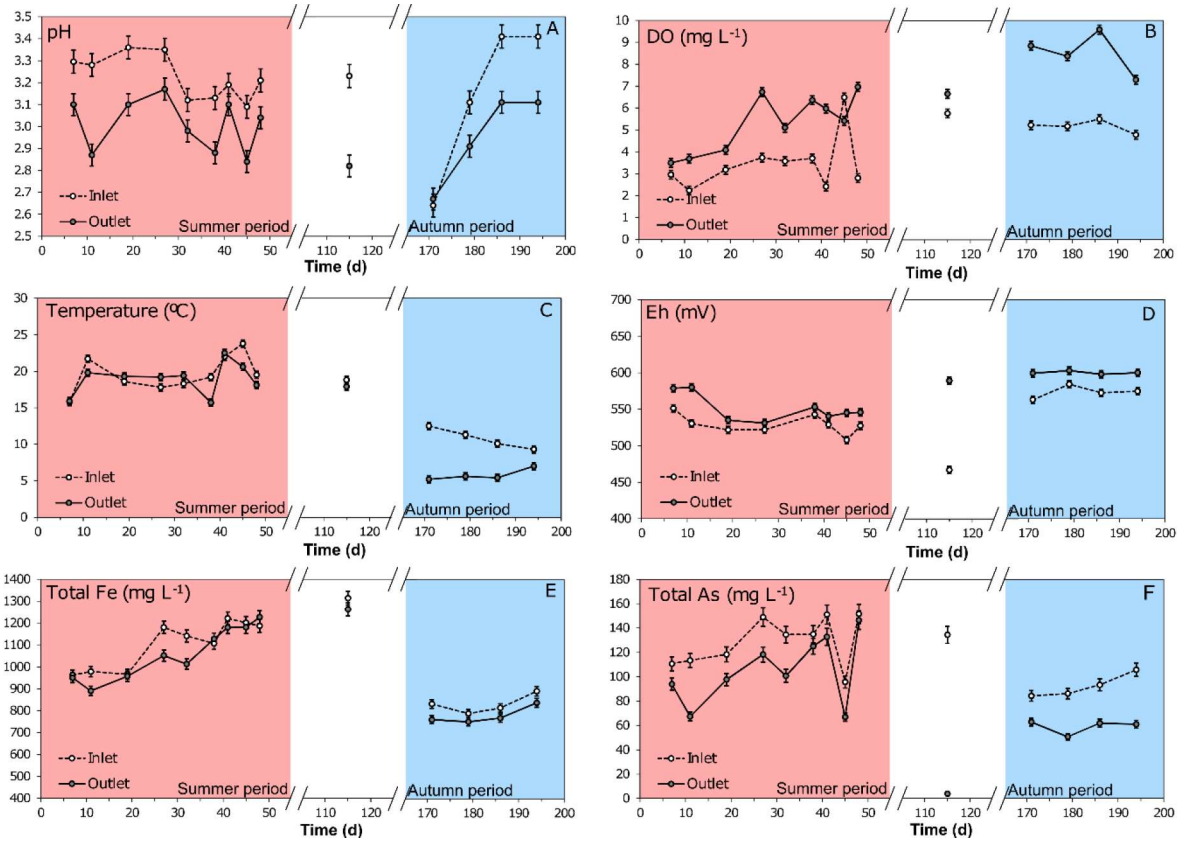

Figure 3. Monitoring of inlet and outlet water pH (A), dissolved oxygen concentration (B), temperature (C), redox potential (D), total dissolved Fe concentration (E), and total dissolved As concentration (F) in the field bioreactor.

Figure 4

Click here to download Figure: 20181014_Figure 4.docx

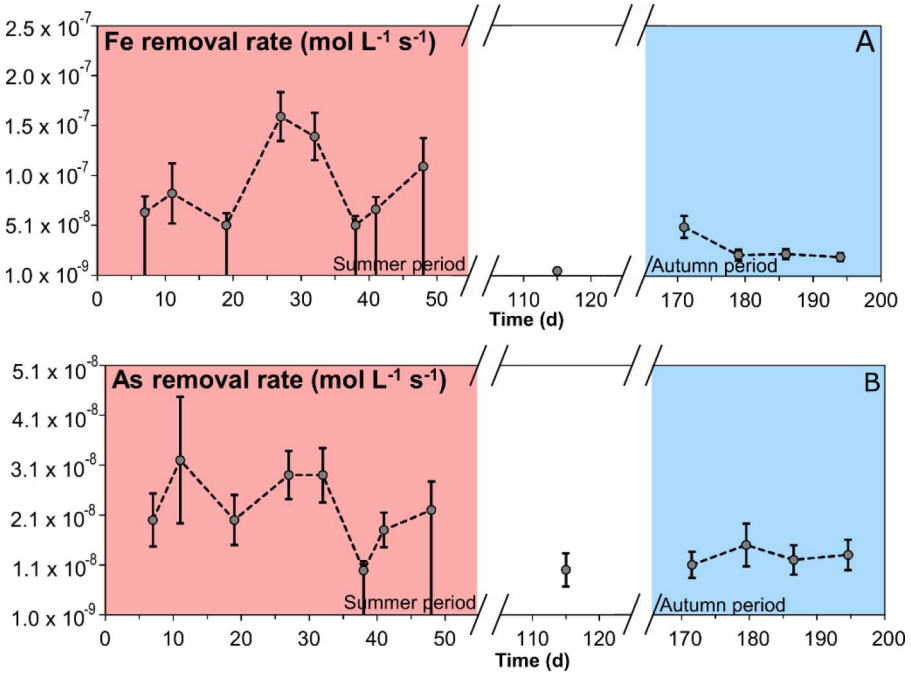

Figure 4. Monitoring of the Fe (A) and As removal rates (B) in the field bioreactor. Rate values represented by a high negative SD correspond to maximum removal rates estimated from the analytical detection limit (no significant total Fe or total As concentration decrease between inlet and outlet).

Figure 5

Click here to download Figure: 20181014_Figure 5.docx

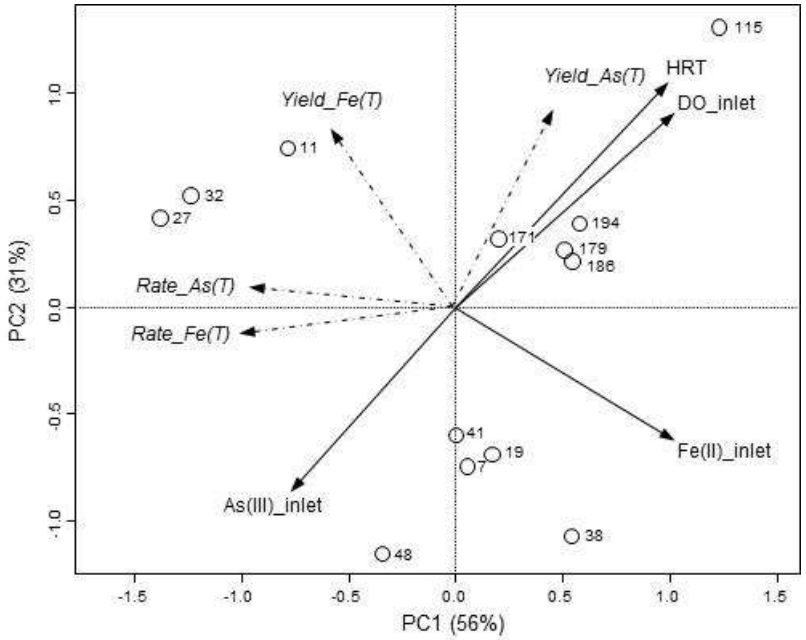

Figure 5. Principal Component Analysis (PC1 × PC2) based on functional parameters (total As and total Fe removal yields and rates) of the bioreactor across time. Circles with numbers represent the sampling days after the bioreactor setup. Vectors in the bi-plot overlay were constructed from a data frame containing HRT and water physico-chemistry parameters (inlet and outlet temperature, DO, pH, Eh, conductivity, Fe and As concentrations and proportions of Fe(II) to total Fe and As(III) to total As). Only correlations with p-values ≤ 0.05 were included. The angle and length of the vector indicate the direction and strength of the variable.

Figure 6
Click here to download Figure: 20181014_Figure 6.docx

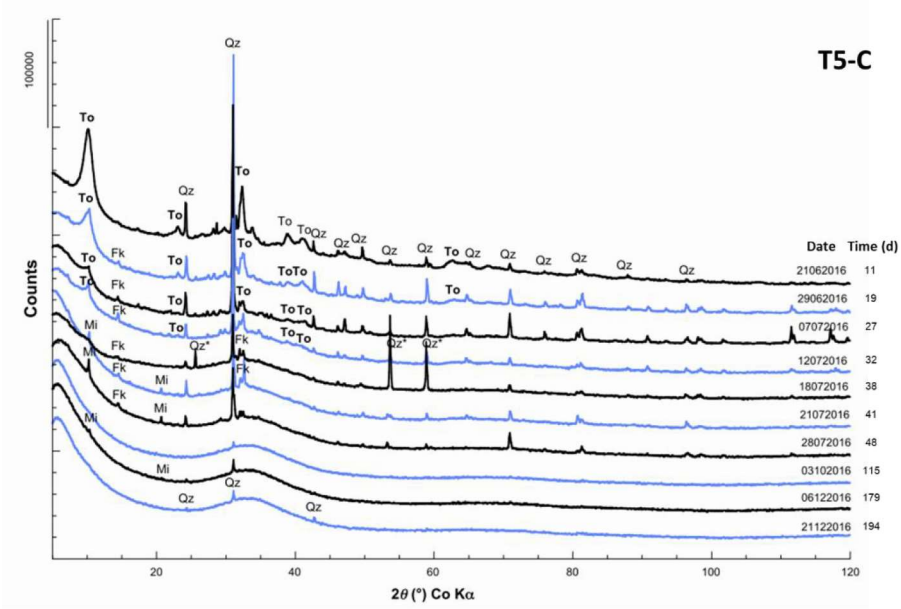

Figure 6. Evolution of X-ray diffractograms on the biogenic precipitate in tray T5-C during the monitoring period. Qz = quartz, To = tooeleite, Fk = potassium feldspar, Mi = micas.

Figure 7
Click here to download Figure: 20181014_Figure 7.docx

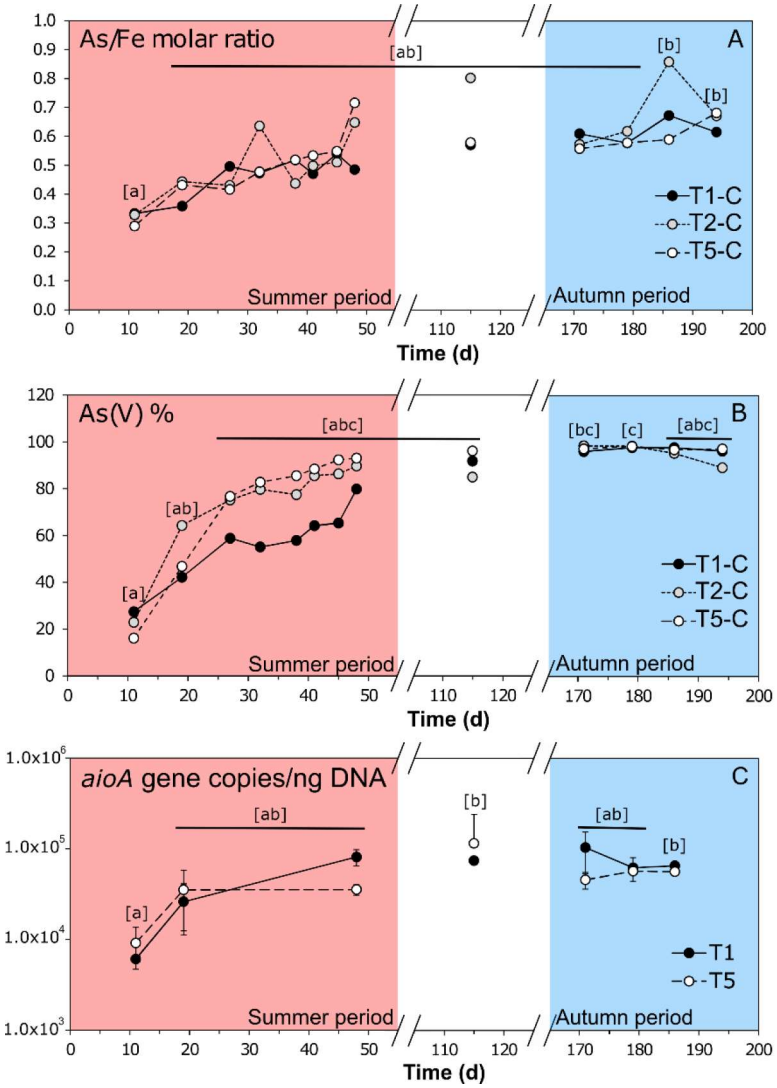

Figure 7. Evolution of As/Fe molar ratio (A) and As(V) percentage (B) in the biogenic precipitate from trays T1-C, T2-C, and T5-C during the monitoring period. Evolution of number of *aioA* gene copies/ng of DNA for trays T1 and T5 (A, B, and C section samples) during the same time (C). Different letters in brackets indicate statistically significant differences according to Friedman (p-value < 0.05) and Nemenyi multiple pairwise comparisons tests.

Table 1
Click here to download Table: 20181014_Table1.docx

Table 1. Comparison with other field trials exploiting biological or chemical Fe precipitation and As removal from AMD water in passive treatment devices

Reference	Site	Whole design	System evaluated	Influent pH	Influent As (mg L^{-1})	Influent Fe (mg L^{-1})	As removal %	Fe removal %	As removal rate (g m^{-2} d^{-1})	Fe removal rate (g m^{-2} d^{-1})	HRT (h)	Mineralogy	As/Fe molar ratio or As concentration in the solid phase
Biological treatments													
This study	Carnoulès mine (France)	5 aerobic ponds stacked on top of each other connected by cascades	Whole system	2.6–3.5	85–150	790–1320	3–97	<0–11	2–13	<0–54	2.3–50	Tooeleite, Amorphous ferric arsenate	0.29–0.86
Elbaz-Poulichet et al. (2006)	Carnoulès mine (France)	Aerobic pond (3 different configurations a) with ridges, b) shallow pond, c) with cascades) + decantation pond (DP) + anaerobic wetland	Aerobic ponds	2.5–4.5	50–250	800–1200	11–20	n.s.	5–10	n.s.	0.5–3	n.s.	n.s.
Macías et al. (2012)	Monte Romero mine (Spain)	Natural iron oxidizing lagoon (NFOL) + dispersed alkaline substrate (DAS) + 2 DP joined by cascades + DAS	NFOL	~3	0.1–1	275 (99 % Fe(II))	80	38	0.1-1*	100*	n.s.	Sch, goe (from Phreeqc calculations)	0.002*
Hamilton et al. (1999)	Wheal Jane mine (UK)	5 aerobic wetlands + anaerobic pond + rock filter	5 aerobic wetlands	~4	2.4	~140	> 99	74	n.s.	1.2	n.s.	n.s.	n.s.
Whitehead et al. (2005)	Wheal Jane mine (UK)	5 aerobic wetlands + anaerobic pond + rock filter	5 aerobic wetlands	3.8	2.7	144	> 99*	75*	n.s.	5.8 (first unit)	n.s.	n.s.	< 0.1 % As (first aerobic cell)
Kalin and Caetano Chaves (2003)	Nova Lima mining district (Brazil)	4 oxidation-precipitation-settling ponds + 3 anaerobic ponds	first oxidation-precipitation-settling pond	2–4	< LD	20–300	n.s.	15–38 (4 aerobic ponds)	~0.004	~11	48	n.s.	~0.0004* (4 aerobic ponds)
Chemical treatments													
Rötting et al. (2008)	Monte Romero mine (Spain)	DAS+ 3 DP joined by cascades	DAS	3.0-3.9	0.1-1.5	290–357 (95 % Fe(II))	99	48 (whole system)	0.05–0.75*	n.s.	24	Sch, goe (0–3 cm depth)	~0.002* (0–3 cm depth)
Caraballo et al. (2009)	Monte Romero mine (Spain)	DAS + 2 DP joined by cascades + DAS + 2 DP joined by cascades + DAS (MgO)	1st DAS	3.08	0.3	358	> 99	34 (1st DAS+ 2 DP)	n.s.	n.s.	24 h	Sch, goe (0–3 cm depth)	n.s.
Gusek et al. (1994)	Leviathan mine (USA)	ALD, 3 aerobic pond, anaerobic pond	Whole system	4.5	0.1	340	90	99	n.s.	n.s.	n.s.	n.s.	n.s.

*Calculated
n.s. = not specified
LD = limit of detection
Sch = schwertmannite, Goe = goethite